Inorg. Chem. **2003**, *42*, 2242−2252

Thermically and Electrochemically Induced Isomerization of a (Bis(ferrocene)−cyclam)copper(II) Complex

Christophe Bucher,[†] Jean-Claude Moutet,*[,†] Jacques Pécaut,[‡] Guy Royal,[†] Eric Saint-Aman,[†] Fabrice Thomas,[§] Stéphane Torelli,[§] and Mihaela Ungureanu[†,||]

Laboratoire d'Electrochimie Organique et de Photochimie Rédox, UMR CNRS 5630, Université Joseph Fourier Grenoble 1, BP 53, 38041 Grenoble Cédex 9, France, DRMFC/SCIB, Laboratoire de Chimie de Coordination, CEA-Grenoble, 17 rue des Martyrs, 38054 Grenoble Cédex 9, France, and Laboratoire de Chimie Biomimétique, LEDSS, UMR CNRS 5616, Université Joseph Fourier Grenoble 1, BP 53, 38041 Grenoble Cédex 9, France

Received October 17, 2002

The new bis(ferrocene)−cyclam macrocycle 1,8-bis(ferrocenylmethyl)-1,4,8,11-tetraazacyclotetradecane, denoted **L**, has been synthesized. Two Cu^{II} complexes with **L** have been isolated and characterized from X-ray structure determination and electrochemical studies. These two **L**Cu^{II} complexes correspond to the type I (ferrocenyl subunits in the same side of the cyclam plane) and type III (ferrocenyl subunits above and below the cyclam plane) isomers. The type I **L**Cu^{II} complex was synthesized from **L** and a Cu^{2+} salt, while the type III isomer was obtained by oxidation in air or by comproportionation of the Cu^{I} complex. The interconversion between type I and type III **L**Cu^{II} complexes is negligible in acetonitrile and slow in dimethyl sulfoxide but fast via an electrochemical reduction−reoxidation cycle. According to UV−vis and electrochemical characterizations, the type III isomer is thermodynamically more stable and the type I isomer is kinetically favored. A type III **L**Ni^{II} complex was also isolated and characterized by X-ray diffraction analysis and from electrochemical studies.

Introduction

The design and the synthesis of functionalized polyazamacrocycles such as 1,4,8,11-tetraazacyclotetradecane (cyclam) remain a subject of intense activity.[1,2] The cyclam framework allows the formation of strong complexes with d- and f-block metal; changes in its substitution pattern act directly on the properties and geometry of the metal complexes and can determine their potential applications.[3−8] In particular, functionalization of cyclam by substituents such as ferrocene has led to a new class of redox-active ligands having wide applications.[9−20] An interesting property of these compounds is their electrochemical recognition ability, which finds application in the development of new chemosensors. The

* To whom correspondence should be addressed. E-mail: Jean-Claude.Moutet@ujf-grenoble.fr. Fax: (33) 04 76 51 42 67.
† UMR CNRS 5630, Université Joseph Fourier Grenoble 1.
‡ CEA-Grenoble.
§ UMR CNRS 5616, Université Joseph Fourier Grenoble 1.
|| Permanent address: Department of Applied Physical Chemistry and Electrochemistry, Politehnica University, Bucharest, Romania.

(1) Denat, F.; Brandes, S.; Guilard, R. *Synlett* **2000**, 561−574.
(2) Lindoy, L. F. *The Chemistry of Macrocycle Ligand Complexes*; Cambridge University Press: Melbourne, Australia, 1989.
(3) Golub, G.; Cohen, H.; Paoletti, P.; Bencini, A.; Messori, L.; Bertini, I.; Meyerstein, D. *J. Am. Chem. Soc.* **1995**, *117*, 8353−8361.
(4) Golub, G.; Zilbermann, I.; Cohen, H.; Meyerstein, D. *Supramol. Chem.* **1996**, *6*, 275−279.
(5) Wagner, F.; Barefield, E. K. *Inorg. Chem.* **1976**, *15*, 408−417.
(6) Jubran, N.; Cohen, H.; Koresh, Y. *J. Chem. Soc., Chem. Commun.* **1984**, 1683−1684.
(7) Corderman, R. R.; Beauchamp, J. L. *J. Am. Chem. Soc.* **1976**, *98*, 3998−4001.
(8) Bakac, A.; Espenson, J. H. *J. Am. Chem. Soc.* **1986**, *108*, 713−719.
(9) Beer, P. D.; Nation, J. E.; McWhinnie, S. L. W.; Harman, M. E.; Hursthouse, M. B.; Ogden, M. I.; White, A. H. *J. Chem. Soc., Dalton Trans.* **1991**, 2485−2492.
(10) De Santis, G.; Fabbrizzi, L.; Licchelli, M.; Mangano, C.; Pallavicini, P.; Poggi, A. *Inorg. Chem.* **1993**, *32*, 854−860.
(11) Tendero, M. J. L.; Benito, A.; Martínez-Máñez, R.; Soto, J.; García-España, E.; Ramírez, J. A.; Burguete, M. I.; Luis, S. V. *J. Chem. Soc., Dalton Trans.* **1996**, 2923−2927.
(12) Padilla-Tosta, M. E.; Martínez-Máñez, R.; Pardo, T.; Soto, J.; Tendero, M. J. L. *J. Chem. Soc., Chem. Commun.* **1997**, 887−888.
(13) Plenio, H.; Aberle, C. *J. Chem. Soc., Chem. Commun.* **1998**, 2697−2698.
(14) Lloris, J. M.; Martínez-Máñez, R.; Pardo, T.; Soto, J.; Padilla-Tosta, M. E. *J. Chem. Soc., Dalton Trans.* **1998**, 2635−2642.
(15) Bellouard, F.; Chuburu, F.; Yaouanc, J.-J.; Handel, H.; Le Mest, Y. *New J. Chem.* **1999**, *23*, 1133−1135.
(16) Beer, P. D.; Bernhardt, P. V. *J. Chem. Soc., Dalton Trans.* **2001**, 1428−1431.
(17) Sancenón, F.; Benito, A.; Hernández, F. J.; Lloris, J. M.; Martínez-Máñez, R.; Pardo, T.; Soto, J. *Eur. J. Inorg. Chem.* **2002**, 866−875.
(18) Benito, A.; Martínez-Máñez, R.; Soto, J.; Tendero, M. J. L. *J. Chem. Soc., Faraday Trans.* **1997**, *93*, 2175−2180.

10.1021/ic020632h CCC: $25.00
Published on Web 03/07/2003

sensing of metal cations is achieved through the perturbation of the redox potential of a ferrocene substituent upon complexation of the free macrocycle. The ferrocene moiety acts as a signaling unit.[9−12,14−17,20] Interestingly, the same strategy could be used for sensing anions—such as phosphate, ATP, sulfate, nitrate, or halide—the host−guest interaction being based on hydrogen bonding between the free or protonated cyclam and the anionic guest.[12,16,18,19] Another interest of these redox ligands is the possible electrochemically induced commutation of their metal complex properties (redox-switching), with perspectives in the area of molecular electronics, multiredox reactivity, catalysis, and biomimetic chemistry.[10,13,15,21,22] It has been shown that the electroactivity of the ferrocene−metallocyclam conjugates can be controlled from the outside (solvent, background electrolyte) and is strongly influenced by a Coulomb-type interaction between the two metal centers.[10,21] Recently a theoretical model, which takes into account the Fe···M^{2+} distance and the relative permittivity of the solvent, has been reported to account for the shift in potential between the free and complexed redox ligand.[18,21,23] It has been elaborated for low permittivity solvents in which the formation of ions pairs has to be considered.[21]

In this paper, we report the synthesis and the characterization of a new ferrocene−cyclam redox macrocycle: 1,8-bis-(ferrocenylmethyl)-1,4,8,11-tetraazacyclotetradecane, **L**, and its Cu^{II} and Ni^{II} complexes. Examples of trans-disubstituted cyclam are rare,[1,24,25] probably because the classical synthetic scheme leading to trans-disubstituted cyclam gives low yields.[26] The synthesis of **L** was performed according to an efficient and straightforward strategy recently reported.[27−29] In the series of cyclam-appended ferrocenes, the most popular is the tetrakis(ferrocenylmethyl)-substituted cyclam.[9,12,14,16−20] Cyclams bearing one[10] and three[17] ferrocenes have been also synthesized and characterized. The only examples of trans-disubstituted ferrocene cyclams consist in a [1 + 1] or [2 + 2] ferrocene-bridged cyclam.[13,21] Dinuclear complexes from a [1 + 2] ferrocene cyclam have been reported.[15] A point of particular interest is the configuration adopted by metal complexes of N-substituted cyclams. The disposition of each substituents, either above or below the coordination plane, gives rise to 16 possible arrangements, which are reduced to the five energetically distinct geometries (types I−V, Figure 1) proposed by Bosnich et al.[30] As an example, the Ni^{II} and Cu^{II} complexes of 1,4,11,8-tetrakis(ferrocenylmethyl)-1,4,8,11-tetraazacyclotetradecane have been isolated in a type I (all the ferrocenylmethyl groups at the same side as the N4 plane) and type III geometry (two substituents above the plane, the two others below the plane), respectively,[20] when only the type I isomer has been reported for Cu^{II} and Ni^{II} complexes with a [1 + 1] ferrocene 1,8-bridged cyclam.[13,21] We describe here the possible interconversion between type I and type III isomers of the Cu^{II} complex with **L**.

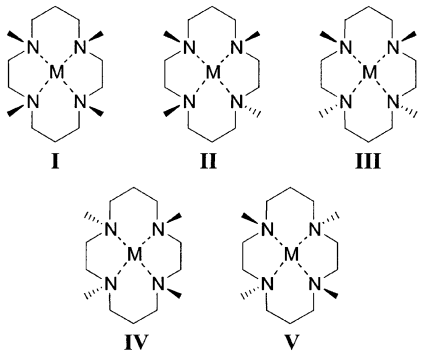

Figure 1. Stereochemistry of metal complexes of cyclam.

Experimental Section

Reagents, Instrumentation, and Procedure. Acetonitrile (Rathburn, HPLC grade) was used as received. Tetra-*n*-butylammonium perchlorate (TBAP) was purchased from Fluka and dried under vacuum for 3 days at 80 °C. Electrochemical experiments were conducted in a conventional three-electrode cell under an argon atmosphere at 20 °C. The reference electrode was $Ag/AgNO_3$ (10 mM in CH_3CN containing 0.1 M TBAP). The potential of the regular ferrocene/ferrocenium (Fc/Fc^+) redox couple in acetonitrile is 0.07 V under our experimental conditions. Rotating disk electrode (RDE) voltammetry was carried out at a rotation rate of 600 rpm. Cyclic voltammetry (CV) curves were recorded at a scan rate of 0.1 V s^{-1}, and the differential pulse voltammetry (DPV) curves were recorded at a 10 mV s^{-1} scan rate with a pulse height of 25 mV and a step time of 0.2 s. The working electrode was a Pt disk (5 mm in diameter for DPV and CV or 2 mm for RDE voltammetry) polished with 1 μm diamond paste before each recording. Electrolysis were performed at controlled potential using a Pt plate and were followed by UV−vis spectroscopy. Electrochemical simulations and best fitting of experimental data were performed using the Electrochemical Simulations Package (ESP software, version 2.4, by Dr. Carlo Nervi (nervi@lem.ch.unito.it)). The diffusion coefficients of all species were fixed at 10^{-5} cm^2 s^{-1}. Diffusion coefficient, electrode surface, viscosity of the electrolytic solution, and concentrations were not fitted. The scale in intensity of the simulated voltammograms is thus arbitrary. The kinetic parameters of the type III $\mathbf{L}Cu^{II}/\mathbf{L}Cu^{I}$ redox couple were determined independently starting from a solution of pure type III $\mathbf{L}Cu^{II}$ in CH_3CN.

(19) Beer, P. D.; Cadman, J.; Lloris, J. M.; Martínez-Máñez, R.; Padilla, M. E.; Pardo, T.; Smith, D. K.; Soto, J. *J. Chem. Soc., Dalton Trans.* **1999**, 127−134.
(20) Tendero, M. J. L.; Benito, A.; Cano, J.; Lloris, J. M.; Martínez-Máñez, R.; Soto, J.; Edwards, A. J.; Raithby, P. R.; Rennie, M. A. *J. Chem. Soc., Chem. Commun.* **1995**, 1643−1644.
(21) Plenio, H.; Aberle, C.; Al Shihadeh, Y.; Lloris, J. M.; Martínez-Máñez, R.; Pardo, T.; Soto, J. *Chem.—Eur. J.* **2001**, *7*, 2848−2861.
(22) Plenio, H.; Aberle, C. *Angew. Chem., Int. Ed. Engl.* **1998**, *37*, 1397−1399.
(23) Beer, P. D.; Cadman, J.; Lloris, J. M.; Martínez-Máñez, R.; Soto, J.; Pardo, T.; Marcos, M. D. *J. Chem. Soc., Dalton Trans.* **2000**, 1805−1812.
(24) Comparone, A.; Kaden, T. A. *Helv. Chim Acta* **1998**, *81*, 1765−1772.
(25) Batsanov, A. S.; Goeta, A. E.; Howard, J. A. K.; Maffeo, D.; Puschmann, H.; Gareth Williams, J. A. *Polyhedron* **2001**, *20*, 981−986.
(26) Lachkar, M.; Andrioletti, B.; Boitrel, B.; Guilard, R.; Atmani, A. *New J. Chem.* **1995**, *19*, 777−779.
(27) Bucher, C.; Duval, E.; Barbe, J.-M.; Verpeaux, J.-N.; Amatore, C.; Guilard, R. *C. R. Acad. Sci., Ser. IIc: Chim.* **2000**, *3*, 211−222.
(28) Bucher, C.; Royal, G.; Barbe, J.-M.; Guilard, R. *Tetrahedron Lett.* **1999**, *40*, 2315−2318.
(29) Royal, G.; Dihaoui-Gindrey, V.; Dahaoui, S.; Tabard, A.; Guilard, R.; Pullumbi, P.; Lecomte, C. *Eur. J. Org. Chem.* **1998**, 1971−1975.
(30) Bosnich, B.; Poon, C. K.; Tobe, M. L. *Inorg. Chem.* **1965**, *4*, 1102−1108.

We found α (transfer coefficient) = 0.74, k^0 (heterogeneous transfer constant) = 10^{-3} cm s^{-1}, and $E° = -0.91$ V, in agreement, in the uncertainty limits, with the best fitting obtained starting from a solution of pure type I **L**Cu^{II} in CH_3CN (see the text). FAB (positive mode) mass spectra were recorded with an AEI Kratos MS 50 spectrometer fitted with an Ion Tech Ltd. gun and using *m*-nitrobenzyl alcohol as matrix. EPR spectra were recorded at 100 K on a Bruker ESP 300E spectrometer operating at 9.4083 GHz (X band; microwave power = 20 mW; modulation amplitude = 0.197 mT) with millimolar solutions of copper(II) complexes in DMSO. Simulated spectra were calculated with the commercially available Bruker Simfonia program. NMR spectra were recorded at 21 °C on a Bruker AC 250. ^{1}H chemical shifts (ppm) were referenced to the solvent deuterium signal. FT-IR spectra (KBr pellets) were recorded on a Perkin-Elmer GX spectrometer. UV−vis spectra were recorded on a Varian Cary 100 spectrophotometer using quartz cells (l = 1 cm). UV−vis measurements vs time for isomerization studies (kinetics and electrolysis experiments) were carried out using a Varian Cary 50 spectrophotometer equipped with a dip probe (l = 1 cm) connected to the spectrophotometer through an optical fiber. Elemental analyses were performed by the Service Central d'Analyses, CNRS, Lyon, France.

Synthesis. 1,8-Dimethyl-4,11-diazoniatricyclo[9.3.1.1^{4,8}]hexadecane (**1**) was prepared as previously reported.[29] (Chloromethyl)ferrocene was prepared by following a procedure similar to that previously described for the synthesis of the 1,1′-bis(chloromethyl)ferrocene, starting from (hydroxymethyl)ferrocene.[15] All reagents and solvents were of reagent grade and used as received.

Synthesis of 1,8-Bis(ferrocenylmethyl)-4,11-diazoniatricyclo-[9.3.1.1^{4,8}]hexadecane Dichloride (2). A 410 mg (1.83 mmol) amount of 1,8-dimethyl-4,11-diazoniatricyclo[9.3.1.1]hexadecane was dissolved in 40 mL of CH_3CN, and 3 molar equiv of freshly prepared (chloromethyl)ferrocene was rapidly added. The resulting solution was stirred overnight at room temperature, and the yellow precipitate formed was filtered off, washed with cold CH_3CN, and dried under vacuum. Yield: 83% (1.05 g). An analytical sample of compound **2** was characterized as its tetrafluoroborate salt, which precipitated on addition of 2.2 equiv of $NaBF_4$ to the chloride salt dissolved in a minimum amount of water. ^{13}C NMR (62.5 MHz, CD_3CN, 298 K) (δ, ppm): 20.2, 30.9, 48.1, 52.1, 60.2, 61.2, 70.3, 71.4, 72.1, 72.9, 73.5, 76.7. FAB$^+$-MS (*m*/*z*): 709 ([**2**,BF_4]$^+$, 100%), 795 ([**2**,$(BF_4)_2$ − H]$^+$, 20%). Anal. Calcd for $C_{34}H_{46}N_4Fe_2B_2F_8$·$H_2O$ (M_r = 814.07): C, 50.16; H, 5.94; N, 6.88. Found: C, 50.18; H, 5.86; N, 6.93.

Synthesis of 1,8-Bis(ferrocenylmethyl)-1,4,8,11-tetraazacyclotetradecane (L). A 300 mg (0.43 mmol) amount of **2** as its chloride salt was dissolved in 100 mL of 3 M aqueous NaOH. After 30 min, the formation of a yellow and oily solid was observed. The mixture was extracted with CH_2Cl_2 (3 × 20 mL), and the organic phases were collected, dried with Na_2SO_4, filtered, and concentrated under vacuum. **L** was obtained as a yellow powder in 96% yield (0.41 mmol, 248 mg). ^{1}H NMR (250 MHz, $CDCl_3$, 298 K) (δ, ppm): 1.74 (m, −NCH_2 *CH_2*CH_2N−, 4H), 2.37 (t, J = 5.5 Hz, −N *CH_2*CH_2CH_2N−, 4H), 2.43 (bs, −NCH_2CH_2 *CH_2*N−, 4H), 2.57 (t, J = 4.75 Hz, −N *CH_2*CH_2N−, 4H), 2.64 (t, J = 4.75 Hz, −NCH_2 *CH_2*N−, 4H), 2.98 (bs, −NH−), 3.50 (s, Fc−*CH_2*−, 4H), 4.09 (m, H_β−Cp, 4H), 4.10 (s, Cp, 10H), 4.14 (m, H_α-Cp, 4H). ^{13}C NMR (62.5 MHz, $CDCl_3$, 298 K) (δ, ppm): 25.4, 47.6, 50.7, 51.4, 52.4, 53.4, 67.8, 68.4, 70.5, 81.4. FAB$^+$-MS (*m*/*z*): 597 ([**L** + H]$^+$, 100%). UV−vis [λ_{max}, nm (ϵ, M^{-1} cm^{-1}); CH_3CN]: 434 (221). Anal. Calcd for $C_{32}H_{44}N_4Fe_2$·H_2O (M_r = 614.424): C, 62.55; H, 7.55; N, 9.12. Found: C, 62.61; H, 7.61; N, 9.27.

Complexes. All metal complexes were synthesized as their perchlorate salt. Warning! Perchlorate salts are hazardous because of the possibility of explosion.

Type I LCu^{II} Complex. Method A. Type I **L**Cu^{II} complex was synthesized at room temperature by mixing stoichiometric amounts of **L** (30 mg, 0.05 mmol) and $Cu(ClO_4)_2$·$6H_2O$ (19 mg, 0.05 mmol) in 5 mL of CH_3OH. A violet precipitate was instantaneously formed, and the mixture was stirred at room temperature for 1 h. The solid was collected by suction filtration, washed with diethyl ether, and dried under reduced pressure (yield: 72%).

Method B. Type I **L**Cu^{II} complex was also prepared upon mixing **L** and $Cu(ClO_4)_2$·$6H_2O$ (0.05 mmol) in 10 mL of degassed CH_3CN. The mixture was stirred under an inert atmosphere for 1 h, and the solid complex was precipitated upon addition of diethyl ether and collected by suction filtration. It was dissolved in cold CH_3CN and crystallized by vapor diffusion of diethyl ether (yield: 63%).

Type I L$Cu(ClO_4)_2$. UV−vis [λ_{max}, nm (ϵ, M^{-1} cm^{-1})]: DMSO, 442 (589), 526 (439, sh); CH_3CN, 467 (694), 511 (614, sh). FAB$^+$-MS (*m*/*z*): 859 ([**L**$Cu(ClO_4)_2$ + H]$^+$, 7%), 758 ([**L**$Cu(ClO_4)$]$^+$, 100%), 659 ([**L**Cu]$^+$, 50%). Anal. Calcd for $C_{32}H_{44}N_4Fe_2Cu$-Cl_2O_8·H_2O (M_r = 876.871): C, 43.83; H, 5.29; N, 6.39. Found: C, 43.61; H, 5.18; N, 6.25.

Type III LCu^{II} Complex. Method A. Type III **L**Cu^{II} complex was prepared at room temperature, in air, upon addition of a stoichiometric amount of $Cu(CH_3CN)_4ClO_4$ (16 mg, 0.05 mmol) into a stirred solution of **L** (30 mg, 0.05 mmol) in 5 mL of CH_3-OH containing an excess of tetra-*n*-butylammonium perchlorate (0.5 mmol). The mixture was stirred for 4 h, and the brown-orange precipitate of type III **L**Cu^{II} complex was filtered off, washed with diethyl ether, and dried under reduced pressure (yield: 58%). It was then dissolved in cold CH_3CN and crystallized by vapor diffusion of diethyl ether.

Method B. Type III **L**Cu^{II} complex was also prepared under an inert atmosphere upon mixing **L** and $Cu(CH_3CN)_4ClO_4$ (0.05 mmol) in degassed CH_3CN (10 mL), via the slow comproportionation of the **L**Cu^{I} complex. The mixture was stirred for 24 h, and the Cu^0 formed was filtered off. Type III **L**Cu^{II} complex was crystallized upon vapor diffusion of diethyl ether into the CH_3CN solution and collected by suction filtration (yield: 25%).

Type III L$Cu(ClO_4)_2$. UV−vis [λ_{max}, nm (ϵ, M^{-1} cm^{-1})]: DMSO, 431 (694); CH_3CN, 460 (723). FAB$^+$-MS (*m*/*z*): 758 ([**L**$Cu(ClO_4)$]$^+$, 100%), 659 ([**L**Cu]$^+$, 50%). Anal. Calcd for $C_{32}H_{44}N_4Fe_2CuCl_2O_8$·$H_2O$ (M_r = 876.871): C, 43.83; H, 5.29; N, 6.39. Found: C, 43.53; H, 5.10; N, 6.25.

Type III LNi^{II} Complex. The **L**Ni^{II} complex was synthesized at room temperature by mixing stoichiometric amounts of **L** (30 mg, 0.05 mmol) and $Ni(ClO_4)_2$·$6H_2O$ (18 mg, 0.05 mmol) in 10 mL of CH_3OH. The mixture was stirred for 2 h, and the yellow precipitate formed was then collected by suction filtration, washed with diethyl ether, and dried under reduced pressure. It was dissolved in cold CH_3CN and crystallized by vapor diffusion of diethyl ether (yield: 53%). UV−vis [λ_{max} (ϵ, M^{-1} cm^{-1})]: DMSO, 411 (470); CH_3CN, 415 (336). FAB$^+$-MS (*m*/*z*): 853 ([**L**$Ni(ClO_4)_2$ + H]$^+$, 25%), 754 ([**L**$Ni(ClO_4)$ + H]$^+$, 100%), 698 ([**L** + ClO_4 + 3H]$^+$, 75%), 654 ([**L**Ni]$^+$, 60%). Anal. Calcd for $C_{32}H_{44}N_4Fe_2$-$NiCl_2O_8$·H_2O (M_r = 872.018): C, 44.08; H, 5.32; N, 6.42. Found: C, 44.53; H, 5.42; N, 6.51.

X-ray Structures. Single crystals of the **L**M^{II} complexes (M = Cu, Ni) denoted respectively **L**Cu^{II} (type I or III) and **L**Ni^{II} were used for data collection on a SMART CCD diffractometer using Mo Kα graphite-monochromated radiation (λ = 0.710 73 Å). Intensity data were corrected for Lorentz, polarization effects, and

Table 1. Crystal Data and Structure Refinement for Type I [**L**Cu]$(ClO_4)_2$, Type III [**L**Cu]$(ClO_4)_2$, and [**L**Ni]$(ClO_4)_2$

	type I [**L**Cu(H_2O)]$(ClO_4)_2$	type III [**L**Cu]$(ClO_4)_2 \cdot 2CH_3CN$	type III [**L**Ni]$(ClO_4)_2$
formula	$C_{32}H_{46}Cl_2CuFe_2N_4O_9$	$C_{36}H_{50}Cl_2CuFe_2N_6O_8$	$C_{32}H_{44}Cl_2Fe_2N_4NiO_8$
fw	876.87	940.96	854.02
cryst system	monoclinic	triclinic	monoclinic
space group	*C*2/*c*	$P\bar{1}$	$P2_1/c$
a (Å)	27.016(2	10.6084(13)	11.166(8)
b (Å)	9.0952(8)	12.0962(14)	8.855(2)
c (Å)	18.1625(15)	16.0326(19)	17.434(15)
α (deg)	90	83.073(2)	90
β (deg)	126.9520(10)	81.848(2)	90.07(8)
γ (deg)	90	75.830(2)	90
V (Å^3)/*Z*	3566.4(5)/4	1966.6(4)/2	1724(2)/2
D_x (g cm^{-3})	1.633	1.589	1.646
μ (cm^{-1})	16.02	14.58	15.83
cryst dimens (mm)	0.3 × 0.5 × 0.5	0.2 × 0.3 × 0.3	0.1 × 0.1 × 0.1
T (K)	293(2)	223(2)	223(2)
θ range for collcn (deg)	2.43−28.95	1.74−28.96	1.82−29.49
no. of rflcns collcd	8834	12 658	4812
data/restraints/params	4093/0/329	8902/3/687	3439/0/311
$R(F)^a$	0.0493 for $I > 2\sigma(I)$	0.0335 for $I > 2\sigma(I)$	0.0386 for $I > 2\sigma(I)$
goodness of fit *S*	0.938	0.967	0.997
$\Delta\rho_{min}/\Delta\rho_{max}$ (e Å^{-3})	0.731/1.020	0.393/0.391	0.584/0.725

[a] $R = \Sigma||F_o| - |F_c||/\Sigma F_o|$.

absorption. Structure solution and refinement were performed with the SHELXTL package. A summary of the crystallographic data and structure refinement is given in Table 1. All non-hydrogen atoms were refined with anisotropic thermal parameters. In **L**Cu^{II} (type I or III), the hydrogen atoms were refined with isotropic thermal parameters. In **L**Ni^{II}, the hydrogen atoms were generated in idealized positions, riding on the carrier atoms with isotropic thermal parameters.

Kinetics. The type I/type III isomerization kinetics of **L**Cu^{II} complexes were followed by UV−vis spectroscopy. Measurements were performed in the 328−358 K temperature range, using millimolar solutions of pure, isolated type I **L**Cu^{II} complex dissolved in degassed DMSO. Determination of the type III to type I molar ratio at equilibrium, which represents the equilibrium constant *K*, was performed by comparison of the UV−vis spectra at equilibrium with the UV−vis spectra of pure type I and III complexes recorded immediately after their dissolution in DMSO at the appropriate temperature. Absorption changes with time were analyzed at 447 nm. Assuming a first-order kinetics for the reactions, the kinetics problem can be expressed as

$$\mathrm{I} \underset{k_{III}}{\overset{k_I}{\rightleftharpoons}} \mathrm{III}$$

$$K = k_I/k_{III} \quad [I] = [I]_0 - x \quad [III] = [III]_0 + x \quad \Delta A = A_t - A_0$$
$$\Delta\epsilon = \epsilon_{III} - \epsilon_I \quad \Delta A = x\Delta\epsilon$$

with

$$x = \{(k_{III}[III]_0 - k_I[I]_0)/(k_I + k_{III})\} \exp(-(k_I + k_{III})t) - (k_{III}[III]_0 - k_I[I]_0)/(k_I + k_{III})$$

where I and III represent the type I and III **L**Cu^{II} isomers, respectively. [], $[]_0$, A_t, and A_0 denote the concentration in type I or III isomer and the absorbance of the solution at the instant *t* and at $t = 0$, respectively. ϵ_I and ϵ_{III} are the absorption coefficients at the selected wavelength of type I and III **L**Cu^{II} isomer, respectively. Using a nonlinear regression method (Kaleidagraph, version 3.0.5), the curves ΔA vs time were fitted to the above expression giving consistent results in all cases and leading to an estimation of $k_I + k_{III}$ and $\Delta\epsilon(k_{III}[III]_0 - k_I[I]_0)/(k_I + k_{III})$. Using the experimental value of *K*, k_I and k_{III} were determined. Furthermore, k_I and k_{III} were also determined from $\Delta\epsilon(k_{III}[III]_0 - k_I[I]_0)/(k_I + k_{III})$ assuming that $k_{III}[III]_0$ is negligeable and using $\Delta\epsilon = 95$ M^{-1} cm^{-1} at 447 nm in DMSO.

Results and Discussion

Synthesis of L. The 1,8-bis(ferrocenylmethyl)-1,4,8,11-tetraazacyclotetradecane **L** was synthesized from the 1,4,8,-11-tetraazatricyclo[9.3.1.1^{4,8}]hexadecane derivative **1** (Scheme 1), following a general and straightforward two-step procedure.[29] Addition of 2 equiv of (chloromethyl)ferrocene to a solution of **1** in CH_3CN resulted in the selective formation of the new disubstituted macrotricycle **2** having two non-adjacent quaternary nitrogen atoms. Due to its ionic character, **2** is insoluble in CH_3CN and was isolated by simple filtration. This intermediate was then hydrolyzed with concentrated aqueous NaOH to yield the aimed macrocycle **L**. It should be noticed that this simple synthetic route proceeds with good yields at room temperature, the compounds being isolated by filtration or extraction.

Synthesis and X-ray Structural Characterization of the Cu^{II} Complexes. When cyclam derivatives coordinate to four equatorial sites of a metal cation, the ligand can adopt five energetically distinct geometries according to the relative orientation of the substituents on each nitrogen (Figure 1), above or below the N4 coordination plane.[30] Two of these arrangements are well-known for Cu^{II} and Ni^{II} complexes of cyclam: the type III isomer with two substituents disposed on each side of the N4 plane and the type I isomer with all four substituents disposed on the same side of the plane.[31] It has been suggested that the type III complex is thermodynamically the more stable isomer and that formation of the type I isomer can occur via a low-energy, kinetically favored pathway.[32] Moreover, it has been shown that interconversion of the (TMC)Ni^{II} (TMC is 1,4,8,11-tetra-

(31) Barefield, E. K.; Freeman, G. M.; Van Derveer, D. G. *Inorg. Chem.* **1986**, *25*, 552−558.
(32) D'Aniello, M. J.; Mocella, M. T.; Wagner, F.; Barefield, E. K.; Paul, I. C. *J. Am. Chem. Soc.* **1975**, *97*, 192−194.

Scheme 1. Synthesis of the Ligand L and Its Copper(II) Complexes

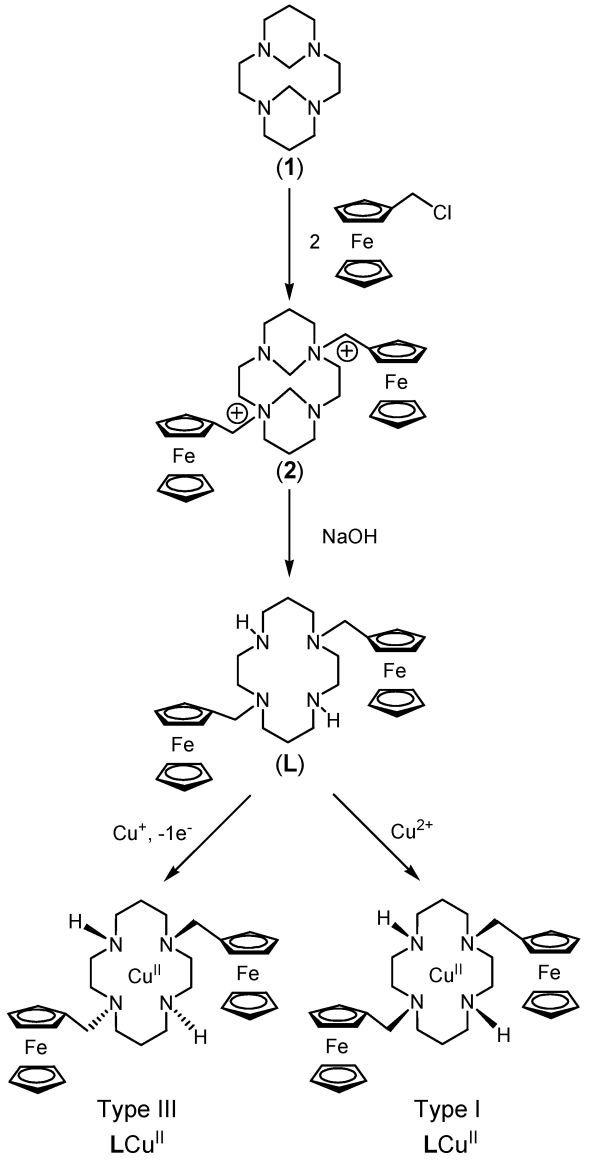

methyl-1,4,8,11-tetraazacyclotetradecane) from type III to type I geometry, via the intermediate type II isomer, occurs rapidly in strongly coordinating solvents such as *n*-propylamine to lead to an equilibrium characterized by a molar ratio type I/type III close to 0.4.[33] Type III to type I conversion of (TMC)Ni^{II} was further confirmed by studies in DMF.[34] Strain-energy minimization analysis by the molecular mechanics method suggested that the type I isomer is preferred for four coordinate complexes, while the type III isomer is preferred for six-coordinate complexes.[35]

Cu^{II} metal complexes of **L** were synthesized at room temperature by reacting stoichiometric amounts of ligand and metal salt. Depending on the experimental conditions (Scheme 1), both type I and type III isomers **L**Cu^{II} were isolated and characterized in the solid state.

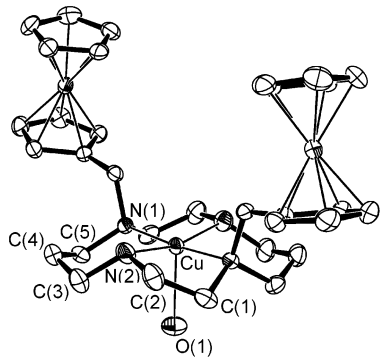

Figure 2. ORTEP view of the type I **L**Cu^{II} isomer showing a partial labeling scheme. Hydrogen atoms have been omitted for clarity. Ellipsoids are drawn at a 40% probability.

A **L**Cu^{II} complex was readily obtained as a violet precipitate when the complexation was performed in CH_3OH. X-ray structure determination showed that it adopts the type I arrangement. Figure 2 shows an ORTEP view of this complex, and selected bond lengths and angles are summarized in Table 2. The molecular structure, $[C_{32}H_{44}N_4Fe_2Cu\cdot H_2O](ClO_4)_2$, consists of a dicationic $[\mathbf{L}Cu]^{2+}$, two ClO_4^- counterions, and one water molecule. The complex crystallizes in the *C*2/*c* space group, revealing a 0.5 crystallographic independent dicationic molecular entity lying on a 2-fold axis passing through the Cu and O(1) atoms. The coordination geometry around the copper cation is best described as a distorted square plane when referring to the cyclam unit alone and as a square pyramid owing to the weak coordination of an additional H_2O molecule (Cu−O(1) = 2.329(4) Å). The Cu−N distances Cu−N(1) and Cu−N(2) are of 2.033(3) and 2.034(3) Å, respectively. The bond angles around the Cu^{2+} center are far from those expected for the ideal square-planar geometry, e.g. angles N(1)−Cu−N(2), N(1)−Cu−N(2A), N(1)−Cu−N(1A), and N(2)−Cu−N(2A) are equal to 93.60(13), 85.67(13), 174.44(15), and 164.7(2)°, respectively. The four nitrogen atoms define a plane within 0.086 Å, and the copper atom is out-of-plane by 0.184 Å. The copper atom and the H_2O molecule lie on the same side of the plane, across the ferrocenyl groups. This contrasts with what has been observed in the case of the type I Ni^{II} complexes of tetraferrocene-substituted cyclam and a [1 + 1] ferrocene-bridged cyclam for which both the coordinated solvent molecule and the bound metal cation are on the same side as the ferrocenyl groups.[13,20,21] No significant distortions are found in the ferrocenylmethyl groups. Cyclopentadienyl rings are almost parallel (tilted angle of ca. 2.9°), and Fe···Cp (centroid) distances are of 1.640 and 1.652 Å, respectively. The intermetallic distances (Fe···Cu = 5.955 Å, Fe···Fe(A) = 9.385 Å, angle Fe···Cu···Fe(A) = 104°) are too long for any direct metal interaction to be invoked.

When the complexation was performed in CH_3OH under aerobic conditions by mixing **L** and Cu^{I} as $Cu(CH_3CN)_4^+$, a brown-orange **L**Cu^{II} complex was formed upon spontaneous oxidation of the copper center by dissolved dioxygen. The X-ray structure determination of this complex, formulated as $[C_{32}H_{44}N_4Fe_2Cu](ClO_4)_2\cdot 2CH_3CN$, revealed that it adopts the type III arrangement (Figure 3 and Table 1). It crystallizes

(33) Moore, P.; Sachinidis, J.; Willey, G. R. *J. Chem. Soc., Chem. Commun.* **1983**, 522−523.
(34) Lincoln, S. F.; Coates, J. H.; Hadi, D. A. *Inorg. Chim. Acta* **1984**, *81*, L9−L10.
(35) Hambley, T. W. *J. Chem. Soc., Dalton Trans.* **1986**, 565−569.

Table 2. Selected Distances (Å) and Bond Angles (deg) for Type I [**L**Cu](ClO$_4$)$_2$, Type III [**L**Cu](ClO$_4$)$_2$, and [**L**Ni](ClO$_4$)$_2$

type I [**L**Cu](ClO$_4$)$_2$[a]		type III [**L**Cu](ClO$_4$)$_2$[b]		type III [**L**Ni](ClO$_4$)$_2$[c]	
Cu−N(1)	2.033(3)	Cu(1)−N(1)	2.0935(18)	Ni−N(1)	1.965(3)
Cu−N(2)	2.034(3)	Cu(1)−N(1)	1.999(2)	Ni−N(2)	1.957(3)
Cu−O(1)	2.329(4)	Cu(2)−N(21)	2.064(2)	N(1)−Ni−N(2)	92.46(11)
N(1)−Cu−N(1A)	174.44(15)	Cu(2)−N(22)	2.002(2)	N(1)−Ni−N(2A)	87.54(11)
N(2)−Cu−N(2A)	164.7(2)	N(1)−Cu(1)−N(1A)	180.000	N(1)−Ni−N(1A)	180.0
N(1)−Cu−N(2)	93.60(13)	N(2)−Cu(1)−N(2A)	180.000	N(2)−Ni−N(2A)	180.00(14)
N(1)−Cu−N(2A)	85.67(13)	N(1)−Cu(1)−N(2)	93.26(8)		
N(1)−Cu−O(1)	92.78(7)	N(1)−Cu(1)−N(2A)	86.74(8)		
N(2)−Cu−O(1)	97.63(11)	N(21)−Cu(2)−N(21B)	180.000		
		N(22)−Cu(2)−N(22B)	180.000		
		N(21)−Cu(2)−N(22)	87.01(9)		
		N(21)−Cu(2)−N(22B)	92.99(9)		

[a] Symmetry equivalent position: A = $-x$, y, $-z + 0.5$. [b] Symmetry equivalent positions: A = $-x + 1$, $-y + 2$, $-z + 2$; B = $-x + 2$, $-y + 2$, $-z + 1$. [c] Symmetry equivalent position: A = $-x + 1$, $-y + 2$, $-z + 1$.

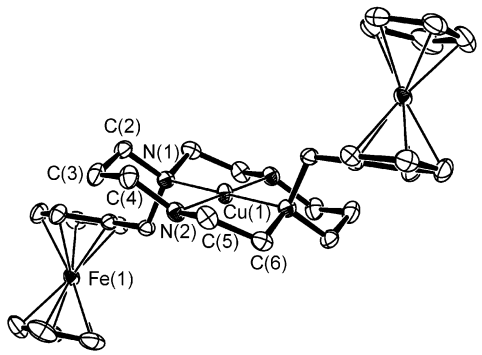

Figure 3. ORTEP view of the type III **L**Cu^{II} isomer showing a partial labeling scheme. Hydrogen atoms have been omitted for clarity. Ellipsoids are drawn at a 40% probability.

in the $P\bar{1}$ space group revealing two crystallographically independent dicationic molecular entities which have an imposed center of symmetry (Cu^{II}). These two entities display very close crystallographic data. The copper environment is provided by the four nitrogen atoms of the cyclam subunit leading to a slightly distorted square-planar coordination geometry. The four nitrogen atoms and the Cu atom define an ideal plane. The angles N(1)−Cu(1)−N(2) and N(1)−Cu(1)−N(2A) are of 93.26(8) and 86.74(8)°, respectively, with Cu−N distances equal to 1.999(2) and 2.0935(18) Å, respectively. No significant distortions are found in the ferrocenylmethyl groups (Cp tilted angle for Fe(1) and Fe(2) of ca. 3.6 and 1.8°, respectively; Fe···Cp distances between 1.632 and 1.649 Å) which lie above and below the N4 plane. The main difference between the two independent entities concerns the geometry of the Cp rings. They are eclipsed around Fe(1) and twisted around Fe(2). As for the type I isomer, the intermetallic distances (Fe(1)···Cu(1) = 6.114 Å, Fe(1)···Fe(1A) = 12.229 Å, angle Fe(1)···Cu(1)···Fe(1A) = 180°) are too long for any direct metal interaction to be invoked.

Complexation turned out to be more complicated when performed in CH_3CN. Indeed, upon addition of Cu(ClO$_4$)$_2$·6H$_2$O to the yellow solution of ligand in CH_3CN, no precipitation occurred and a blue color typical of the formation of ferrocenium species developed. Cu^{2+} is a strong oxidant in CH_3CN and is thermodynamically capable to oxidize **L** and its Cu^{II} complexes, leading to a mixture of

Table 3. EPR Spectra of Type I and Type III **L**Cu^{II} Complexes Recorded in Frozen DMSO (100 K) Solution (A_{xx}, A_{yy}, A_{zz} in G)

	type I **L**Cu^{II}	type III **L**Cu^{II}		type I **L**Cu^{II}	type III **L**Cu^{II}
A_{xx}	20	20	g_{xx}	2.042	2.031
A_{yy}	36	28	g_{yy}	2.064	2.067
A_{zz}	187	192	g_{zz}	2.187	2.189

Table 4. Electrochemical Data[a] for Free Ligands and **L** + Cu^{II} or Ni^{II} Complexes

	LCu^{II}		**L**Ni^{II}		
L: Fc/Fc$^+$	Fc/Fc$^+$	Cu^{II}/Cu^{I}	Fc/Fc$^+$	Ni^{II}/Ni^{I}	Ni^{II}/Ni^{III}
0.125	0.21[b]	−0.83,[c] −0.91[d]	0.20	−1.41	1.08

[a] $E_{1/2}$ (V) vs Ag/0.01 M AgNO$_3$ measured in CH_3CN electrolyte. [b] No difference in the $E_{1/2}$ according to the configuration of the complex. [c] Type I **L**Cu^{II}. [d] Type III **L**Cu^{II}.

(**L**)$^{n+}$Cu$^{I/II}$ species (n = 1 or 2). It should be noticed that the redox potential of the complexed Cu^{I}/Cu^{II} couple is lower than that of the ferrocene/ferrocenium (Fc/Fc$^+$) couple in the free or complexed ligand (Table 4). Therefore, the back transfer of one electron from Cu^{I} to Fc$^+$ can occur and, under argon, the **L**Cu^{II} complex was almost quantitatively formed in a few minutes as judged from UV−visible measurements. Under aerobic conditions, the intermediate Cu^{I} species can be in part oxidized by dissolved dioxygen into Cu^{II} species prior to the back electron transfer and the resulting solution contains a mixture of **L**Cu^{II}, (**L**)$^+$Cu^{II}, and (**L**)$^{2+}$Cu^{II} complexes. Mixing **L** and Cu(CH$_3$CN)$_4$ClO$_4$ in degassed CH_3CN solution under an inert atmosphere led also to the type III **L**Cu^{II} complex (see Experimental Section), via the slow comproportionation of the **L**Cu^{I} complex according to the reaction 2**L**Cu^{I} → **L** + Cu^0 + **L**Cu^{II}, leading to a low yield in **L**Cu^{II} (25%).

The different reactions can be summarized as

$$\mathbf{L} + \mathrm{Cu^{II}} \xrightarrow{\mathrm{CH_3OH}} \text{type I } \mathbf{L}\mathrm{Cu^{II}} \text{ (fast precipitation)}$$

$$\mathbf{L} + \mathrm{Cu^{II}} \xrightarrow{\mathrm{CH_3CN,\ Ar}} \text{type I } \mathbf{L}\mathrm{Cu^{II}}$$

$$\mathbf{L} + \mathrm{Cu^{II}} \xrightarrow{\mathrm{CH_3CN,\ O_2}} \text{mixture of } \mathbf{L}\mathrm{Cu^{II}} \text{ and } (\mathbf{L})^{n+}\mathrm{Cu^{II}}\ (n = 1 \text{ or } 2)$$

$$\mathbf{L} + \mathrm{Cu^{I}} \xrightarrow{\mathrm{CH_3OH,\ O_2}} \text{type III } \mathbf{L}\mathrm{Cu^{II}} \text{ (precipitation)}$$

$$\mathbf{L} + \mathrm{Cu^{I}} \xrightarrow{\mathrm{CH_3CN}} {}^1/_2\mathrm{Cu^0} + {}^1/_2 \text{ type III } \mathbf{L}\mathrm{Cu^{II}} + {}^1/_2\mathbf{L}$$

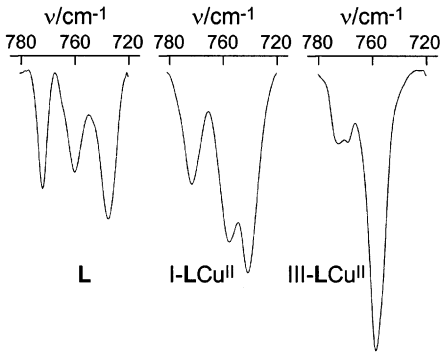

Figure 4. FT-IR spectra of free **L**, type I **L**Cu^{II}, and type III **L**Cu^{II}.

While the type I copper(II) complex is obtained upon complexation of **L** with Cu^{2+}, the type III isomer can be prepared via the oxidation of the Cu^{I} complex. It can be assumed that different coordination modes around the copper center according to its redox state are responsible for the formation of the two different isomers. This will be further confirmed from electrochemical results.

FT-IR Characterization of the LCu^{II} Complexes. The type I and III **L**Cu^{II} complexes are distinguishable in the solid state, thanks to their FT-IR features. The most consistent variations are in the 720−780 cm^{-1} region (Figure 4). The signature of the type I isomer is a series of weak vibrational bands at 734, 749, and 767 cm^{-1}, while the IR spectrum of the type III isomer shows only two bands at 747 and 763 cm^{-1}. It is of interest to note that the spectrum of the type I **L**Cu^{II} reveals very marked similarity to that of the free ligand **L**, which presents three bands at 730, 749, and 767 cm^{-1} (Figure 4). It can be thus reasonably assumed that the free ligand **L** adopts the same conformation as the kinetically favored type I **L**Cu^{II} complex.

EPR Characterization of LCu^{II} Complexes. Type I and type III **L**Cu^{II} complexes dissolved in DMSO (100 K) displayed typical EPR spectra of square-planar Cu^{II} complexes (in the distortion limit) with copper hyperfine structure. From the simulation were obtained the parameters listed in Table 3. Despite the lack of nitrogen hyperfine structure, spectra recorded for type I and type III **L**Cu^{II} strongly suggest the presence of only one species in solution in each case. Moreover, the EPR parameters calculated for these two complexes indicate a similar coordination geometry around the copper center.

Type I−Type III Isomer Thermal Interconversion. Since type I and type III isomers of **L**Cu^{II} display different UV−vis features (Figure 5), their possible interconversion was investigated from UV−vis experiments using millimolar solutions of complex prepared by dissolution of pure type I or type III isomers in CH_3CN or in DMSO. At room temperature (288−298 K) and in both solvents, no significant changes in their respective UV−vis spectra could be observed after 24 h; i.e., the rearrangement is negligeable or extremely slow under these experimental conditions. The same observation was made when the temperature of CH_3CN solutions was raised to 343 K. On the contrary, upon increase of the temperature in DMSO, the type I **L**Cu^{II} turned out to rearrange to the type III isomer and vice versa (Figure 5A). An equilibrium was reached after several hours, even at elevated temperature (e.g. 12 h at 343 K). The isomerization process was then studied in the temperature range 328−358 K. As judged from careful analysis of the UV−vis spectra, the same equilibrium position was reached starting from either pure type I complex or pure type III complex. It is characterized by a type III on type I molar ratio of ca. 13:1, without any significant variation in the studied temperature range. The major product thus adopts the commonly believed most stable type III configuration in DMSO solution. Starting from the type I **L**Cu^{II} complex, the absorption band appearing as a shoulder at 526 nm gradually decreased in intensity as the absorption band located at 431 nm, characteristic of the type III isomer, gradually increased. An isosbestic point was observed at 505 nm (Figure 5A). Monitoring changes vs time in the UV−vis spectra of type I isomer allowed us to estimate the rate of interconversion, k_I, of type I into type III in DMSO. Values of $10^5 k_I$ equal to 3.3, 7.2, and 24 s^{-1} were found at T = 328, 343, and 358 K respectively, with $k_I/k_{III} = 13$ and an activation energy equal to 62.3 kJ mol^{-1}.

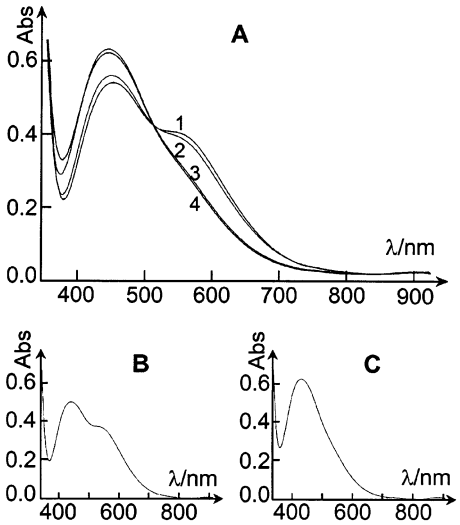

Figure 5. (A) UV−vis spectra of type I **L**Cu^{II} (8.9 mM) recorded in DMSO vs time at 343 K: t = 0 (1), 2 (2), 12 (3), and 14 h (4). Insert: UV−vis spectra of (B) type I **L**Cu^{II} (8.5 mM) and of (C) type III **L**Cu^{II} (9.0 mM) recorded in DMSO at 293 K. l = 1 cm.

Electrochemical Investigations. The electrochemical behavior of the free ligand **L** in CH_3CN solution studied by cyclic voltammetry (CV), rotating disk electrode (RDE) voltamperometry, or differential pulse voltammetry (DPV) is characterized by a single two-independent-electron, reversible process at an apparent $E_{1/2} = 125 \pm 5$ mV ($\Delta E_p = 65$ mV) corresponding to the ferrocene/ ferrocenium (Fc/Fc^+) redox couple. This ΔE_p value strongly suggests that the two chemically equivalent ferrocenyl groups in **L** are electrochemically independent. In the specific case of molecules containing two chemically equivalent, noninteracting redox centers, it has been indeed established that the voltammograms exhibit the shape observed for a single electron-transfer reaction, i.e. a single CV wave with a peak to peak separation close to 58 mV, and that the expected difference

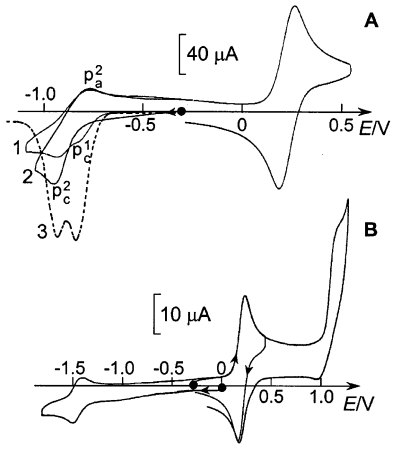

Figure 6. Voltammetric curves at Pt disk electrode (5 mm in diameter) in CH_3CN + 0.1 M TBAP of (A) **L**Cu^{II} (curves 1 and 3, type I, 1.5 mM; curve 2, type III, 2 mM) and (B) **L**Ni^{II} (0.3 mM). CV (A, curves 1 and 2, and B): scan rate 0.1 V s^{-1}. DPV (A, curve 3): scan rate 10 mV s^{-1}; pulse height 25 mV; step time 0.2 s; *E* vs Ag/10 mM Ag^+ + 0.1 M TBAP in CH_3CN.

between the two formal potentials is 35.6 mV (at 297 K).[36] The measured $E_{1/2}$ is thus an average of the two formal potentials for the two redox centers.

CV curves of the isolated **L**Cu^{II} complexes are shown in Figure 6A, and their electrochemical data are summarized in Table 4. In both complexes the potential of the Fc/Fc^+ redox couple is higher than in the free ligand ($\Delta E_{1/2} = +85$ mV) and independent of the type I or type III configuration. This positive shift is attributed to electrostatic repulsions arising between the bound cation and the electrogenerated positive charge on the oxidized ferrocenyl subunits, leading to a destabilization of complexes in their Fc^+ form. However, the potential shift is relatively small because the intermetallic $Fe\cdots M^{II}$ distance is rather large (ca. 6 Å at solid state) in this nonconjugated framework, which prevents the establishment of a strong electrostatic repulsion. Assuming that there is no electronic communication through bonds between the ferrocenyl group and the bound metal cation, the electrochemical shift, ΔE (mV), induced by the complexation event can be theoretically calculated[18,21,23] by taking into account the sole free energy associated with the electrostatic repulsion according to

$$\Delta E = \frac{1}{jn}\left[\frac{14398}{\epsilon}\sum_j\sum_i \frac{1}{r_{ji}} + \left(\frac{2\times 10^6}{\epsilon^2} + 1051\right)\sum_j\sum_i \frac{1}{r_{ij}^2}\right]$$

where *j* is the number of redox groups, *n* the number of electrons, ϵ the macroscopic relative permittivity of the medium, and *i* the number of substrate at a r_{ji} (Å) distance from the redox center. Using $\epsilon = 37.5$ and $r_{ji} \cong 6$ Å for the two **L**Cu^{II} complexes, a theoretical value close to 65 mV is deduced, in accordance with the experimental values. Moreover, in agreement with this model, no significant difference in the extent of the potential shift could be expected according to the configuration of the metal complexes, since type I and type III copper complexes present very similar intermetallic $Fe\cdots M$ distances in the solid state.

The cathodic response of the complexes shows a large stabilization of the +II oxidation state of the metal cation (Table 4). It is worth noting that different cathodic responses are observed for type I and type III copper complexes (Figure 6A). The CV curve for the type III copper complex is characterized by a quasi-reversible redox peaks system (p_c^2 and p_a^2) at $E_{1/2} = -0.91$ V (Figure 6A, curve 2). In contrast, the CV curve for the type I isomer shows two cathodic peaks and one anodic wave (Figure 6A, curve 1). Two well-behaved reduction peaks are seen on the corresponding DPV curve, at $E_p = -0.825$ and -0.905 V (Figure 6A, curve 3). Judged from coulometric measurements and by comparison of the heights of the RDE waves for these redox couples to that of the Fc centers, the overall copper-centered reduction process in the type I isomer corresponds to a one-electron transfer. Moreover, the 2nd reduction peak and the reoxidation peak (curve 1) match with those for the type III complex (curve 2). Obviously the 1st reduction peak (p_c^1) corresponds to the electrogeneration of the type I **L**Cu^I complex that undergoes a fast rearrangement (at the CV time scale) to form the type III **L**Cu^I. Since the potential corresponding to the generation of type I **L**Cu^I species is more positive than the redox potential of the $Cu^{II/I}$ system in the type III complex, type III **L**Cu^I species are immediately reoxidized into type III **L**Cu^{II} species which are then reduced at a more negative potential (peak p_c^2). The overall electrochemical mechanism can be modeled as a classical square scheme involving both the electron-transfer reactions (type I and III **L**Cu^{II}/**L**Cu^I redox couples) and the isomerization processes undergone by **L**Cu^{II} and **L**Cu^I. However, taking into account the very slow kinetics and the "quasi" irreversibility of the **L**Cu^{II} isomerization process, the square scheme can be approximated to the following mechanism:

$$\text{I } \mathbf{L}Cu^{II} + e^- \rightleftarrows \text{I } \mathbf{L}Cu^{I} \quad E^\circ = -0.832 \pm 0.012 \text{ V}$$
$$\alpha = 0.53 \pm 0.12 \quad k^0 = 5 \times 10^{-3} \text{ cm s}^{-1}$$

$$\text{I } \mathbf{L}Cu^{I} \rightarrow \text{III } \mathbf{L}Cu^{I} \quad k = 1.15(\pm 0.15) \times 10^4 \text{ s}^{-1}$$

$$\text{III } \mathbf{L}Cu^{II} + e^- \rightleftarrows \text{III } \mathbf{L}Cu^{I} \quad E^\circ = -0.914 \pm 0.017 \text{ V}$$
$$\alpha = 0.79 \pm 0.04 \quad k^0 = 10^{-3} \text{ cm s}^{-1}$$

Here α and k^0 are the apparent transfer coefficient and the apparent heterogeneous transfer constant of the corresponding electrochemical reaction. The characteristic constants of this mechanism have been determined by simulating the voltammetric behavior of type I **L**Cu^{II} as a function of the scan rate. The low values found for k^0 and the high values found for α suggest that the electron-transfer steps are more complicated than a simple heterogeneous electron transfer. They indeed involve adsorption steps (revealed from RDE experiments; see below) and solvation reorganization processes. The main conclusion concerns the high value found for the kinetic constant *k* ($1.15(\pm 0.15) \times 10^4$ s^{-1}), which confirms that the type I to type III isomerization in the **L**Cu^I complex is a fast process, the type I **L**Cu^I complex having

(36) Flanagan, J. B.; Margel, S.; Bard, A. J.; Anson, F. C. *J. Am. Chem. Soc.* **1978**, *100*, 4248−4253.

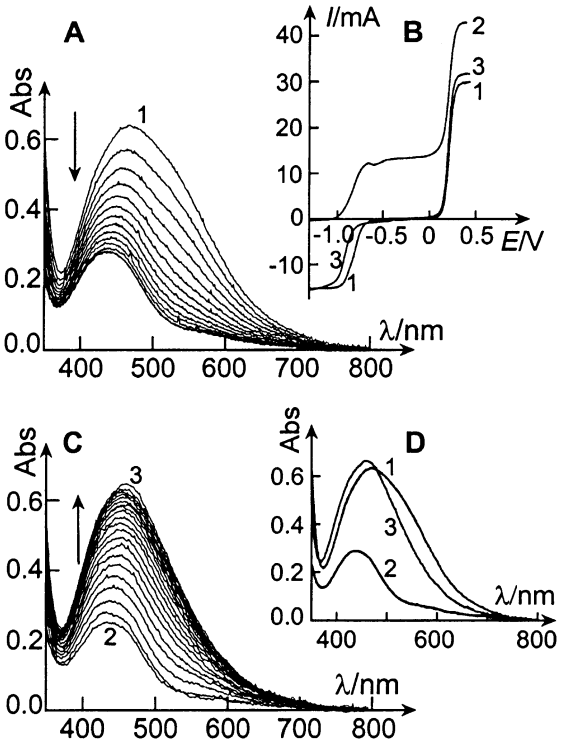

Figure 7. UV−vis spectra ($l = 1$ cm) of a $CH_3CN + 0.1$ M TBAP solution of type I **L**Cu^{II} (1.0 mM): (A) during reduction at −1.4 V; (C) during reoxidation at −0.4 V. Insert (D): curve 1, initial; curve 2, after reduction at −1.4 V; curve 3, after reoxidation at −0.4 V. (B) Corresponding voltammetric curves at a Pt RDE (600 rpm, 2 mm in diameter): *E* vs Ag/10 mM $Ag^+ + 0.1$ M TBAP in CH_3CN.

an apparent half-life of ca. 60 μs. The speed of the reductively induced type I/type III interconversion in the (bis-(ferrocene)−cyclam)copper(II) complex is thus similar to that already observed with (TMC)Cu^{II} [37] or penta- and hexa-coordinated cyclam-based copper complexes.[27]

The potentials of the Cu^{II}/Cu^{I} redox couple in type I and type III **L**Cu^{II} complexes (−0.83 and −0.91 V, respectively) indicate that the +II redox state of the bound copper atom is slightly stabilized in the type III isomer as compared to the type I isomer, suggesting a more thermodynamically favorable coordination of Cu^{II} in the complex of the former configuration.

Type I to type III electrochemically induced isomerization was further examined by potentiostatic exhaustive electrolysis coupled with UV−vis spectroscopy (Figure 7). Exhaustive reduction at $E_{app} = -1.4$ V of a solution of pure type I **L**Cu^{II} complex consumed 1.01 electron/molecule and led to the quantitative generation of **L**Cu^{I} complex ($\lambda_{max} = 411$ nm, $\epsilon = 283$ M^{-1} cm^{-1}, Figure 7A), as evidenced by the heights of the RDE voltammetry waves recorded before (Figure 7B, curve 1) and after (Figure 7B, curve 2) electrolysis. Weak adsorption phenomena are responsible for a "pseudopolarographic" maximum on the RDE wave (see Figure 7B, curve 2), precluding an accurate determination of $E_{1/2}$ of the reduced complex. Exhaustive reoxidation of this solution at $E_{app} = -0.4$ V gave the **L**Cu^{II} complex with the type III configuration (Figure 7B,C). Isomerization of the complex is clearly evidenced by the significant changes in the UV−visible spectra recorded before (Figure 7D, curve 1) and after (Figure 7D, curve 3) the reduction−reoxidation cycle. The spectrum of the final solution compares well with that of pure type III **L**Cu^{II} complex. Type I to type III conversion is further corroborated by the negative potential shift of the $Cu^{II/I}$ reduction wave, from −0.83 V in the initial solution (Figure 7B, curve 1) to −0.91 V (Figure 7B, curve 3) in the final solution. This isomerization could be explained by a fast change in the coordination sphere around the bound metal cation upon its reduction, the sole stable configuration of the Cu^{I} complex probably being energetically close to the type III geometry. On the other hand, exhaustive oxidation at +0.5 V of a solution of the type I **L**Cu^{II} complex consumes 1.94 electron/molecule and led to the quantitative formation of $(\mathbf{L})^{2+}Cu^{II}$ ($\lambda_{max} = 628$ nm, $\epsilon = 916$ M^{-1} cm^{-1}). Upon exhaustive reduction at −0.2 V of this solution, the starting type I **L**Cu^{II} complex is fully restored; i.e., no isomerization was observed. Given the 9 Å Fc···Fc distance in type I **L**Cu^{II}, no electrostatic repulsion able to force the isomerization process can take place between the two Fc^+ moieties in $(\mathbf{L})^{2+}Cu^{II}$.

Synthesis and Characterization of Ni^{II} Complexes. To evaluate the influence of the nature of the complexed metal cation on the isomerization process, we carried out a similar study with the **L**Ni^{II} complex. As a matter of fact, the oxidatively induced isomerization of the type I (cyclam)Ni^{II} into type III complex has been previously reported,[38] this process being energetically favored and kinetically faster with nickel center in its +III oxidation state. The corresponding kinetic constant appeared lower than in the case of cyclam-based copper complexes, leading to the observation of two distinguishable reversible CV waves (in the 0.2−1 V s^{-1} range) for the two (cyclam)Ni^{II} isomers.

Isolation of the complex **L**Ni^{II} could be easily achieved upon recrystallization in CH_3CN + diethyl ether of the powder obtained from precipitation of $Ni(ClO_4)_2 \cdot 6H_2O$ + **L** in CH_3OH. The crystal structure of this complex reveals a type III stereochemistry (Tables 1 and 2). The Ni^{II} complex, formulated as $[C_{32}H_{44}N_4Fe_2Ni](ClO_4)_2$, crystallizes in the $P2_1/c$ space group of the monoclinic system, revealing a 0.5 crystallographically independent dicationic molecular entity which has a center of inversion (Ni^{II}). The Ni^{II} environment in **L**Ni^{II} is close to that of Cu^{II} in the type III **L**Cu^{II}. The four nitrogen atoms and the Ni atom define an ideal plane with angles N(1)−Ni−N(2) and N(1)−Ni−N(2A) equal to 92.46(11) and 87.54(11)°, respectively. The N−Ni bond lengths are equal to 1.965(3) Å (N(1)−Ni) and 1.957(3) Å (N(2)−Ni). The ferrocenyl groups are characterized by a tilted angle of 3.0(2)°, and the Fe···Cp (centroid) distances are equal to 1.638(2) and 1.648(2) Å. The intermetallic distances Fe···Ni and Fe···Fe(A) are of 5.853 and 11.706 Å, respectively (angle Fe···Ni···Fe(A) = 180°).

However, FT-IR experiments strongly suggest the formation of at least two isomers in the course of the synthesis of

(37) Bucher, C.; Duval, E.; Espinosa, E.; Barbe, J.-M.; Verpeaux, J.-N.; Amatore, C.; Guilard, R. *Eur. J. Inorg. Chem.* **2001**, 1077−1079.

(38) Pierce, D. T.; Hatfield, T. L.; Billo, E. J.; Ping, Y. *Inorg. Chem.* **1997**, *36*, 2950−2955.

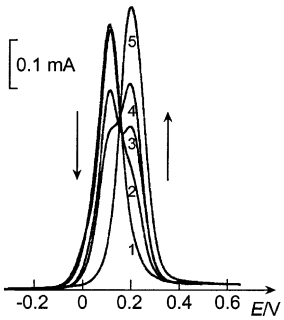

Figure 8. Titration by DPV at Pt disk electrode (5 mm in diameter) of **L** (0.9 mM) with $Ni(ClO_4)_2 \cdot 6H_2O$: scan rate 10 mV s^{-1}; pulse height 25 mV; step time 0.2 s; $Ni^{II}/\mathbf{L} = 0$ (curve 1), 0.23 (curve 2), 0.45 (curve 3), 0.67 (curve 4) and 1.00 (curve 5); *E* vs Ag/10 mM $Ag^+ + 0.1$ M TBAP in CH_3CN.

the $\mathbf{L}Ni^{II}$ complex. Whereas the IR spectrum of the isolated type III isomer presents only two weak bands (749 and 770 cm^{-1}) in the 720−780 cm^{-1} region, the formation of at least another isomer was evidenced by the presence of an additional band at 735 cm^{-1} in the spectrum of the filtrate collected after precipitation of the complex. Unfortunately, crystallization of the crude product recovered upon evaporation of the filtrate gave always the sole type III isomer, suggesting that a rearrangement occurs during the crystallization process of $\mathbf{L}Ni^{II}$. Moreover, thermal interconversion starting from type III $\mathbf{L}Ni^{II}$ could not be performed since decomposition of the complex is observed upon heating.

The electrochemical behavior of $\mathbf{L}Ni^{II}$ was then studied. Since only one isomer (type III) was isolated and characterized, no study on a possible electrochemically induced change of configuration could be attempted. The cyclic voltammetry curve for the $\mathbf{L}Ni^{II}$ complex in CH_3CN is depicted in Figure 6B, and the corresponding redox potentials are given in Table 4. As already observed with the $\mathbf{L}Cu^{II}$ complexes, the Fc/Fc^+ redox couple in the nickel complex is higher than in the free ligand ($\Delta E_{1/2} = +75$ mV), due to electrostatic repulsions arising between the bound cation and the electrogenerated positive charge on the oxidized ferrocenyl subunits. It has to be noted that, in agreement with the theoretical model, no significant difference in the extent of the potential shift could be expected according to the nature of the +2 bound metal cations since copper and nickel complexes present very similar intermetallic Fe···M distances. In addition to the Fc/Fc^+ redox couple, two reversible waves attributed to the $Ni^{II/I}$ ($E_{1/2} = -1.41$ V) and $Ni^{II/III}$ ($E_p = +1.08$ V) redox couples are observed.

Sensing Properties of L toward Cu^{II} and Ni^{II} Cations. Complexation of **L** with Cu^{II} or Ni^{II} was also followed by examining the evolution of the electrochemical response of the redox macrocycle in the presence of various amounts of metal cations. Upon addition of increasing amounts of Cu^{II} or Ni^{II} in CH_3CN electrolytic solutions of **L**, the electrochemical response of the complexed redox macrocycle rose gradually. In particular, a new redox wave due to the Fc/Fc^+ redox couple in the complexed ligand grew at the expense of the original wave for the free ligand (Figure 8). Moreover, RDE voltammetric curves shown that the bis(ferrocene)−cyclam ligand can be oxidized by Cu^{2+}, as evidenced by the appearance of wave of weak intensity corresponding to the reduction of ferrocenium species. Oxidation of the free ligand or of the copper complex thus parallels the complexation. Due to its strong oxidizing character in CH_3CN, free Cu^{2+} (0.65 V under our experimental conditions, determined from RDE voltammetry) is thermodynamically capable to oxidize both the free ligand and its Cu^{II} complex into their ferrocenium forms. These results corroborate the observations made in the course of the synthesis of the copper complexes in acetonitrile.

The small potential shift between the complexed and the free Fc/Fc^+ centers results in a partial overlapping of the two corresponding CV waves, but a good resolution in two peaks was obtained in DPV experiments (Figure 8). The maximal perturbation is reached at a molar ratio M^{II}/ligand equal to 1, corresponding to the stoichiometry of the complex. Analysis of the voltammetric curves as a function of the amount of added cations allows the amperometric titration of the guest. This result confirms the ability of the ferrocene-substituted cyclam to sense transition metal cations.[11,12,18−21]

Conclusion

A new ferrocene cyclam redox macrocycle 1,8-bis(ferrocenylmethyl)-1,4,8,11-tetraazacyclotetradecane, **L**, has been synthesized using a simple and efficient strategy. This ligand completes the cyclam-appended ferrocene series among which only the mono-, tri- and tetraferrocene-substituted cyclam were known. The Cu^{II} and Ni^{II} complexes with **L** have been isolated. The type I (ferrocenyl subunits in the same side of the cyclam plane) and type III (ferrocenyl subunits above and below the cyclam plane) $\mathbf{L}Cu^{II}$ isomers have been characterized from X-ray structure determination. Only, the type III $\mathbf{L}Ni^{II}$ complex could be isolated. The type I $\mathbf{L}Cu^{II}$ complex was prepared from a mixture of **L** and Cu^{II} when the type III isomer could be synthesized upon oxidation in air or by comproportionation of the Cu^{I} complex. Thus, we studied the interconversion between two stable isomers of $\mathbf{L}Cu^{II}$ which had not been evidenced with other (ferrocene−cyclam)metal complexes. The interconversion between type I and type III $\mathbf{L}Cu^{II}$ complexes was shown to be negligible in acetonitrile, slow in DMSO, but fast upon an electrochemical reduction−reoxidation cycle. According to UV−vis and electrochemical characterizations, the type III isomer is thermodynamically more stable and the type I isomer is kinetically favored.

As already observed with other cyclam-appended ferrocene derivatives, the redox potential shift of the Fc/Fc^+ group, upon complexation with a M^{2+} metal cations, is weak and lower than 100 mV. This is explained by considering the $Fc\cdots M^{2+}$ distance too large to allow strong electrostatic repulsion to be established between the +2 charge on the bound metal cation and the electrogenerated positive charge on the Fc center. However, this shift might be exploited for sensing transition metal cations from DPV experiments. Since the bis(ferrocene)−cyclam ligand **L** can be further

functionalized at its two "free" N positions, work is in progress to try to improve its sensing properties by grafting appropriate complexing groups on the macrocycle. Additional functionalizations in **L** might be also of interest to modulate redox-induced configuration changes in its corresponding metal complexes.

Supporting Information Available: X-ray data in CIF format for type I **L**Cu^{II}, type III **L**Cu^{II}, and type III **L**Ni^{II} and experimental and simulated X-band EPR spectra of type III **L**Cu^{II} and type I **L**Cu^{II} complexes. This material is available free of charge via the Internet at http://pubs.acs.org.

IC020632H